

Cite this: *RSC Adv.*, 2016, 6, 52236

The effect of structural heterogeneity on the conformation and stability of A β -tau mixtures†

Hyunsung Choi,‡^a Myeongsang Lee,‡^a Harold S. Park*^b and Sungsoo Na*^a

Oligomeric and fibrillar amyloids, which cause neurodegenerative diseases, are typically formed through repetitive fracture and elongation processes involving single homogeneous amyloid monomers. However, experimental and computational methods have shown that the amyloid proteins could be composed of heterogeneous amyloid segments. Specifically, owing to the polymorphism of amyloids under physiological conditions, it is crucial to understand the structural characteristics of heterogeneous amyloids in detail by considering their specific mutations and polymorphic nature. Therefore, in this study we used atomistic simulations to reveal the various structural characteristics of heterogeneous amyloids, which are amyloids composed of amyloid beta (A β) and mutated tau proteins. Furthermore, we showed that the different characteristics and conformations of A β -tau mixtures are the cause of the different types of tau proteins based on A β segments. Interestingly, we found that valine and lysine residues have a significant impact on the structural conformation and stability of the heterogeneous A β -tau mixtures. We also showed that two types of binding are key to understanding the different binding features and mechanical reactions to tensile load. This study sheds light on the assembly features of heterogeneous A β -tau mixtures as neurodegenerative disease factors.

Received 12th April 2016

Accepted 20th May 2016

DOI: 10.1039/c6ra09467h

www.rsc.org/advances

1. Introduction

Amyloidogenic proteins are the hallmark of pathological neurodegenerative disorders such as phenylketonuria and Alzheimer's, Parkinson's, Huntington's, and prion-related diseases.^{1–4} Such proteins make a key contribution to neurodegenerative diseases and exist *in vivo* in various forms such as fibers, oligomers, and plaques. Fibrillar amyloids are frequently observed from experimental studies using atomic force microscopy, transmissible electron microscopy, scanning electron microscopy, cryo-electron microscopy, *etc.*^{5–7} Owing to the non-degradable characteristics of fibrillar amyloids, many attempts have been made to determine the structures of fibrillar amyloid proteins. Recently, the importance of oligomeric amyloid structures has emerged; not only do oligomeric amyloids act as seeds that develop into fibrillar amyloids or amyloid plaques, but they also have toxic characteristics under physiological conditions.^{8–10} In particular, the toxic characteristics of oligomeric amyloids have been proven through membrane permeation, deletion of the lipid bilayer, and inflammatory reaction phenomena.⁸ Thus, it is important to

understand the formation and structural characteristics of oligomeric amyloids.

Many attempts have been made to determine the toxic characteristics of amyloid oligomers and fibers, and the mechanisms underlying their formation from single-unit monomers. For instance, Collins *et al.* reported the intermediate progression from oligomeric to fibrillar Sup35 amyloids through repetitive additions of monomer, oligomeric elongations, and fragmentations.¹¹ Xue *et al.* revealed that the biological properties of fragmented amyloid fibrils, which comprise fragmented amyloid proteins, have a toxic effect on cell viability and are involved in the deletion of the membrane lipid bilayer.¹² Furthermore, the fibrillar or oligomeric growth phenomena of amyloid monomers were observed under various physiological conditions including pH, ionic strength, and presence of metal ions.^{6,13–16} For example, different environmental conditions induce diverse formations of transthyretin (residues 105–115) amyloid protofibrils, which change according to lateral thickness composition.^{17–19} The polymorphic characteristics of oligomeric amyloids that arise from different environmental segments have also been reported.^{20–23} Moreover, several experimental groups have investigated the role of specific metal ions on oligomeric and fibrillar amyloid formations, and found that specific metal ions accelerate the formation of amyloid beta (A β) oligomeric amyloids.^{15,24–27} Specific residue-mutated segments also have an effect on the formation of amyloids. For example, computational and experimental investigations of particular mutated residues, or the solvent

^aDepartment of Mechanical Engineering, Korea University, Seoul 02841, Republic of Korea. E-mail: nass@korea.ac.kr

^bDepartment of Mechanical Engineering, Boston University, Boston, MA 02115, USA. E-mail: parkhs@bu.edu

† Electronic supplementary information (ESI) available. See DOI: 10.1039/c6ra09467h

‡ These authors (H. C. and M. L.) contributed equally to this work.

effects at salt-bridge regions and central hydrophobic core (CHC) regions, have shown that mutated residues alter the structural conformations and characteristics of A β amyloid proteins.^{28–34}

However, although an understanding of oligomeric single-amyloid proteins is crucial, determining the cross-seeding effects on oligomeric and fibrillar amyloid growth is also important. Generally, the agents of Alzheimer's disease are considered to be aggregated A β amyloid tangles (*i.e.*, oligomers, fibers, and plaques), which are generated by the proteolytic activation of beta amyloid precursor protein (APP) at membranes.⁸ However, after proteolytic processing of beta amyloid precursor protein from membranes, these APP proteins have an effect on tau proteins in the microtubules of human brains, causing the detachment of tau proteins from microtubules and inflammatory reactions.^{35,36} Subsequently, these APP proteins combine with tau proteins, which act as seeds, forming fibrillar forms and plaque structures. This “cross-seeding” phenomenon affects fibrillar growth. Based on these cross-seeding development phenomena, Guo *et al.* reported insoluble mixtures of the oligomeric form of A β and tau proteins in Alzheimer's disease.³⁷ They used western blotting to determine the specific binding sites between the C-terminal region of A β and tau proteins. Ono *et al.* also investigated the cross-seeding effects of A β and α -synuclein proteins based on different amounts of additional individual amyloid proteins.³⁸ Similarly, Seeliger *et al.* reported the heterogeneous interaction between hIAPP and A β amyloid proteins at lipid membranes.³⁹ Interestingly, Pinotsi *et al.* directly observed heterogeneous amyloid fibril growth by single alpha-synuclein protein structures through two-color super-resolution microscopy.⁴⁰ They reported that homogeneous elongation depends on the particular α -synuclein amyloid at the ends of the protein seed for each different direction. Under physiological conditions, not only did single monomers of amyloids develop into oligomeric and fibrillar amyloid proteins, but heterogeneous amyloid proteins were also found to grow into oligomeric and fibrillar amyloid structures.

To understand in detail the cross-seeding effects of heterogeneous oligomeric amyloids, computational methods have been applied to each individual heterogeneous amyloid protein.^{41,42} For example, Miller *et al.* used replica-exchange molecular dynamics (REMD) and Monte Carlo methods to investigate heterogeneous tau and A β amyloid proteins based on the β -turn- β motif.⁴³ They suggested synergistic interactions between A β and polymorphic structures of tau protein using equilibrated MD simulations of different partial tau protein regions.⁴² Moreover, despite applying the different heterogeneous types of amyloid from the computational study conducted by Miller *et al.*, Berhanu *et al.* reported different amyloid compositions in hIAPP and A β proteins through equilibrated MD study.⁴⁴ Recently, Zheng *et al.* reported different oligomeric amyloid compositions in hIAPP and A β amyloid proteins using multi-scale MD simulation including equilibrated MD and coarse-grained MARTINI MD simulations.⁴⁵ Using combined MD studies, they reported that the double layer and elongation models of cross-seeding structures are stable. Likewise,

understanding heterogeneous amyloid protein in detail is important because it has different structural characteristics. Recently, using combined computational and experimental methods, Miller *et al.* and Shea *et al.* have reported various structural compositions resulting from the specific deletion of the 280th residue in the R2 region of the tau protein (Δ K280).^{44,46} They investigated the polymorphic characteristics of the R2 region of the tau protein by deleting the K280 residue and adding additional residues (*i.e.*, lysine and proline). The deletion of the K280 residue and the addition of other residues affected the structural stability of the tau proteins because the lysine residue is a charged amino acid. Furthermore the researchers also reported the possible existence of heterogeneous A β -tau protein mixtures varying in tau component content (*i.e.*, R2, R3, and R4). However, the effects of polymorphic R2 tau structures, which are composed of Δ K280 and additional residues, still need to be determined to understand the heterogeneous cross-seeding mechanism. Considering that oligomeric A β amyloid proteins together with tau proteins are crucially related to Alzheimer's disease, it is also important to investigate the structural characteristics of heterogeneous interactions between A β and polymorphic R2 tau protein structures in terms of the different effects of hydrophobicity arising from Δ K280 and additional residues.

In this study, we investigated the structural characteristics of heterogeneous interactions between A β and tau protein structures based on polymorphic tau structures by considering the effects of Δ K280 and additional residues. We also constructed two different binding models of heterogeneous A β -tau oligomeric mixtures to understand the different binding mechanisms of heterogeneous interactions, referring to binding mechanisms previously suggested by Pinotsi *et al.*, Shvadchak *et al.*, and Xu *et al.*^{40,47,48} By using combined MD and steered molecular dynamics (SMD) techniques, we have provided comprehensive insights into the heterogeneous structural characteristics of mutated tau and A β amyloid oligomers. We have also suggested various oligomeric characteristics of heterogeneous mixtures and different binding features between mutated tau and A β oligomeric structures for the two elongation types.

2. Material and methods

2.1. Construction of heterogeneous A β and tau structures

To compose the heterogeneous A β and tau structures, we used Lührs model of A β_{17-42} and the second repeat part (²⁷⁵R2³⁰⁵) of full-length tau protein structures. Basically, because both the A β_{17-42} and ²⁷⁵R2³⁰⁵ tau structures from previous studies share the common β -turn- β motif, we used Lührs model of A β_{17-42} for structure construction, with Protein Data Bank symbol 2BEG.²⁹ Here, we considered A β_{17-42} as a template for seeds because A β structures detach the full-length tau proteins from binding to microtubules. Lührs *et al.* conducted multiple structural models from the A β_{17-42} structures determined by NMR investigations.²⁹ The ²⁷⁵R2³⁰⁵ tau regions, which are known to have the most stable interactions with A β_{17-42} proteins, were considered in this study, referring to studies by Miller *et al.*^{41,42}

For the construction of the $^{275}R2^{305}$ tau proteins, we followed previous computational and experimental studies, which found those proteins to be stable. Additionally, in the present study, we suggest another model for $^{275}R2^{305}$ tau oligomers using the first and second structure from Lühr's model. By replacing the tau residues on the second structure of Lühr's model, we were able to observe the hydrophobic effect of interior and exterior valine residues on the $^{275}R2^{305}$ tau oligomers. To distinguish between internal and external valine residue locations in the wildtype $^{275}R2^{305}$ tau oligomers, we denoted them WT1 and WT2, respectively.

Before building up the various A β -tau oligomeric structures, we differentiated between the two types of binding in the A β -tau mixtures by considering the experimental results reported by Pinotsi *et al.* As mentioned in the previous section, we assumed that A β_{17-42} assumed the role of the seed, which act as the reference structure. Based on this assumption, we constructed the top of the tau structure and the bottom of the A β structure, which was designated 'T1'. The 'T2' model is the reverse of the 'T1' model in that the tau model was constructed at the bottom section while the A β model was located at the top section. The structural configurations of the T1 and T2 models are described in Fig. 1(a).

To construct the T1 model, eight layers of A β were initially stacked up. Four top layers were then placed into tau sequences using the Visual Molecular Dynamics (VMD) "mutator" plugin. We also constructed the mutated model of $^{275}R2^{305}$ tau by following previous tau computational and experimental models such as M1, M31, and M41.⁴¹ Using this process, we excluded M2, M32, and M42 models owing to the loss of stability resulting from the change in the number of hydrogen bonds from Raz *et al.*⁴¹ The M1, M31 and M41 models were generated to obtain the same mutating methods to compare them with the wildtype tau models. M1 was constructed based on the prepared wildtype $^{275}R2^{305}$ tau model by deleting the K280 residue ($\Delta K280$). After the $\Delta K280$ procedure, the remaining void residue region was filled by shifting the rest of the C-terminus sequence

residues towards K280. The M31 model is generated by extending the tail of the C-terminal part of the $^{273}R2^{305}$ tau sequence by adding one proline residue (P301) to the M1 model. The M41 model was generated by extending the tail of the N-terminal of the $^{275}R2^{305}$ tau protein by adding one lysine residue (K274). Based on these construction processes, we denoted the models WT1T1, WT2T2, M1T1, M31T1, and M41T1. The remaining T2 binding model was modeled in the same way as the T1 model. The basic cross-sections of each A β -tau are represented in Fig. 1(b).

2.2. Molecular dynamics (MD) simulations protocol

After composing both wildtype and mutated heterogeneous A β -tau structures, the GROMACS 4.6.5 program with the CHARMM27 force field was used to construct the heterogeneous A β -tau mixtures.⁴⁹ Total structural energies of oligomers were minimized using the steepest descent method for 10 000 steps. After that, they were solvated explicitly with TIP3P water molecules in a triclinic box, with a boundary distance of 15 Å for each side of the water box. All of the water molecules within 2.5 Å of the A β -tau oligomers were removed. Counter ions were added to neutralize the net charge of the A β around the structure. A temperature of 330 K was maintained using the Berendsen thermostat algorithm. The short-range van der Waals interactions were computed using the switching function, with a twin range cut-off of 10.0 and 12.0 Å. Long-range electrostatic interactions were computed using the particle mesh Ewald method with a cutoff of 12.0 Å. The leapfrog integrator was used for the equations of motion as an integrator, with a time-step of 2 fs. The solvated system energies were minimized, and then equilibrium simulations were computed with NVT and NPT ensembles for 100 ps during each step (in NVT ensembles, amount of atom (N), volume (V), and temperature (T) are conserved; in NPT ensembles, N , pressure (P), and T are conserved). All the atoms were constrained and the SHAKE

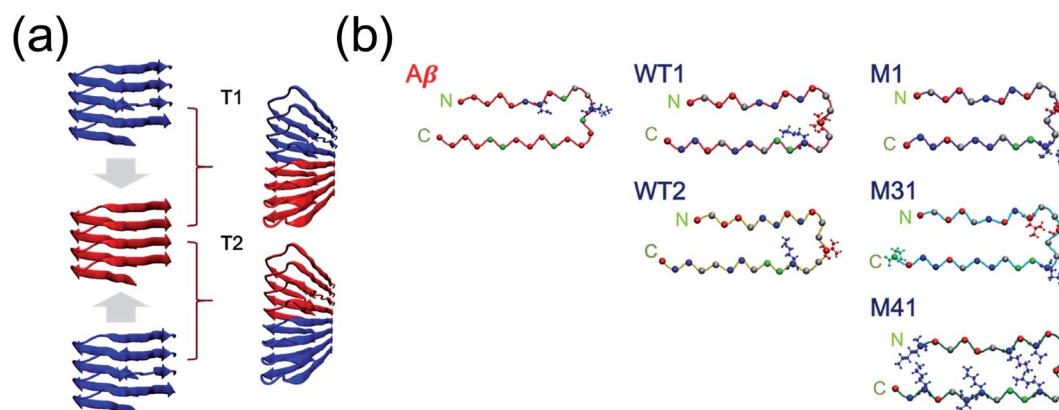


Fig. 1 (a) A scheme of possible binding site for monomers. Upper and lower monomers (blue) are indicating tau monomers and A β monomer is represented at middle (red). T1 and T2 refer to the different binding types, which are upper binding (T1) and beneath binding (T2), respectively. (b) The cross-sectional configurations of simulation models are represented. The names of A β monomers are written in red and the name of tau monomers are written in blue. The shape of beta-turn-beta is drawn with tube and sphere by VMD program. Alpha carbons of each layers are described with color spheres. Red sphere indicate hydrophobic characteristic, blue means hydrophilic characteristic, silver represents special residues and green sphere indicate uncharged residues.

algorithm was applied for the constraint algorithm. All the MD simulations were run for 20 ns at 330 K with the NPT ensemble.

2.3. Structural characteristic analysis of heterogeneous A β -tau

To investigate the structural stability of the heterogeneous A β -tau oligomer mixture after equilibrium MD simulation, we used root mean square deviation (RMSD), the number of hydrogen bonds, and Poisson–Boltzmann surface area (MM/PBSA) analysis.⁵⁰ For the structural conformation analysis, RMSD was measured using the *g_rmsd* plugin of the GROMACS program. Subsequently, to investigate the structural characteristics of the A β -tau oligomer, MM/PBSA and the number of hydrogen bonds were measured using *g_hbonds* and *g_mmpbsa* plug in of GROMACS. For the RMSD and the number of hydrogen bonds, data for each model were obtained over the entire 20 ns period. Specifically, the MM/PBSA method was applied to evaluate the stabilities of interactions between stabilized heterogeneous mixtures for the stacked directions using the *g_mmpbsa* plugin of the GROMACS 4.5.6 program. MM/PBSA analysis configurations were extracted every 1 ps. The binding energy for the MM/PBSA calculations was given by the following equation:

$$\Delta G_{\text{binding}} = G_{\text{mixture}} - (G_{\text{A}\beta} + G_{\text{Tau}}) \quad (1)$$

here, G_{mixture} is the total free energy of the A β -tau mixture, and $G_{\text{A}\beta}$ and G_{Tau} represent the isolated total free energies in solvent, respectively. The total free energy was computed using the following equation:

$$G_{\text{monomer}} = \langle E_{\text{MM}} \rangle + \langle G_{\text{solvation}} \rangle \quad (2)$$

where G_{monomer} represents either the A β , tau, or A β -tau mixture, $\langle E_{\text{MM}} \rangle$ is the average molecular mechanics (MM) potential energy *versus* time, which comprises bond, bond angle, dihedral, and non-bonded energies, and $\langle G_{\text{solvation}} \rangle$ represents the solvation free energy for the entire MD simulation. Since entropic terms are ignored for calculation of the total free energy for monomers, the calculated solvation free energy represents the relative, rather than the absolute, energy. Even though we did not consider the entropic contribution to the calculation of energy, the summation of the total contribution of entropic terms to the system was quite small. Therefore we ignored those terms in the calculation of the total solvation energy.^{50–52} Using the MM/PBSA method, the solvation free energy can be calculated using the two terms below:

$$G_{\text{solvation}} = G_{\text{PB}} + G_{\text{nonpolar}} \quad (3)$$

where G_{PB} and G_{nonpolar} are distinguished by electrostatic effects on the solvation free energy. G_{PB} was estimated using the Poisson–Boltzmann equation,⁵⁰ whereas G_{nonpolar} was computed using the following equation:

$$G_{\text{np}} = \gamma \times \text{SASA} + \beta \quad (4)$$

This equation can be used with the parameters of $\gamma = 0.0226778 \text{ kJ mol}^{-1} \text{ \AA}^{-2}$ and $\beta = 3.84928 \text{ kJ mol}^{-1}$. Solvent

accessible surface area (SASA) was obtained using the *g_sas* tool of the GROMACS program for each model.

2.4. Steered molecular dynamics (SMD) simulations protocol

To support the conformational stability of the heterogeneous A β -tau oligomer results from equilibrium MD, and to understand the structural characteristics, SMD simulations were performed using GROMACS 4.6.5 with CHARMM27 force field. Tensile tests of A β -tau oligomers were performed to determine the properties of the different heterogeneous oligomer compositions, *via* time–force results. During the tensile test simulations, A β monomers were fixed and tau monomers are pulled under conditions of constant velocity by mimicking the atomic force microscopy tensile test. The pulling rate for constant velocity was 0.001 nm ps^{-1} and the spring constant was $1000 \text{ kJ mol}^{-1} \text{ nm}^{-2}$, using the NPT ensemble. During the analysis of the time–force trajectories, we extracted the configuration data for the A β -tau oligomers every 2 ps.

3. Results and discussions

3.1. Conformational characteristics of heterogeneous A β -tau models

In this study, the WT and mutated heterogeneous A β -tau models including different amyloid binding characteristics (*i.e.*, T1 and T2), were computed for comparisons of the structural stabilities and their characteristics. WT models and mutated (M1, M31, and M41) models including different binding types were prepared to investigate the impact of different sequences on the stabilities of heterogeneous interactions. The characteristics of the heterogeneous A β -tau oligomers, including the detailed sequences and the amino acids features of each model, are given in Tables S1 and S2.† A β monomers are regarded as seeds that have two binding sites for elongation, attaching tau along the fibril axis, as shown in Fig. 1(a). Here, only parallel inter-layer interactions based on β -turn- β motif between heterogeneous monomers are considered, because parallel heterogeneous interactions are more stable than anti-parallel inter-layer interactions.⁴³ These stable parallel and unstable anti-parallel characteristics were computationally investigated by Raz *et al.*, who computed the possible structural compositions of A β and tau oligomers.⁴³ The dominant differences between the two binding types, T1 and T2, are described in detail in Fig. S2.† Fig. 2(a) depicts an exact comparison of the T1 and T2 models viewed along the same fibril axis. Those two differently constructed oligomers look like mirror images of each other, and their cross-sectional representations are shown in Fig. S1.†

Through the equilibrium MD simulations we found that each heterogeneous A β -tau mixture become stable after 15 ns, as shown in Fig. 4 and 6 (see initial 0 ns time-section). Some mutated models showed relatively higher or lower structural stability compared with the WT models, which may have been caused by the structural fluctuation near the N- and C-terminal regions. The stabilities of the heterogeneous A β -tau mixtures

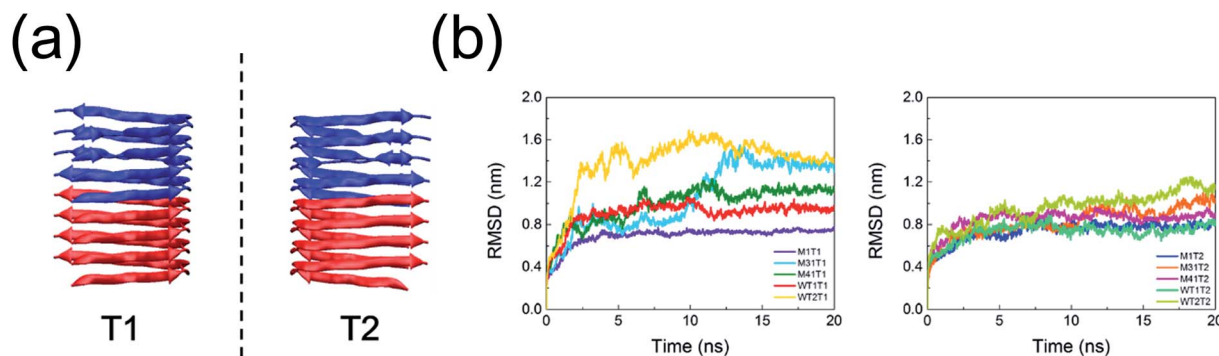


Fig. 2 (a) A scheme for the oligomers, which are stacked along the different directions (T1 and T2). The root mean squared deviation (RMSD) values are plotted for each simulation models at (b).

were confirmed by RMSD analysis, as shown in Fig. 2(b). All models converged after approximately 15 ns, having different convergent values. The results can be compared with previous computational mutated proteinaceous material studies. Most of the RMSD results gradually converged. The total deformations were approximately 2–4 Å. Some models of A β -tau structures (*i.e.*, M1 and WT1) were deformed from the beginning, but there were notably big deformations in the conformational results and RMSD graphs (*i.e.*, Fig. 2 and 4). However, rapid changes of RMSD were observed in the WT2T1, M41T1, and M31T1 models. Especially, M31T1 model undergoes the little conformational change at 10–12 ns period, in which degradation of beta-turn-beta motif at tau region was observed. The results are comparable to the results of previous conformational analyses, which were conducted to determine the end terminal fluctuation behavior of the oligomers. In particular, the WT2T2 model was considerably deformed during the early time period, and the breakage of the two top layers of the tau protein region was observed from the beginning of the equilibration simulation. The exterior-located lysine residues appeared to induce breakage by electrostatic repulsion. However, the interior hydrophobic regions contracted to reduce the number of water molecule within a few picoseconds, thereby stabilizing the interior region. Here, we classified the hydrophobic and hydrophilic residues of A β and tau mixtures following the hydropathy scale measurement of Kyte *et al.*⁵³ More hydrophobic and hydrophilic residue information was classified in ESI Table S2[†] in detail. This interior stabilization was not observed in the M31T1 model, as reflected in the RMSD graphs (left graphs in Fig. 2(b) around 10 ns over two steps). This may have been affected by the proline residue, which acts as a beta-sheet breaker at the N-terminal of M31T1. It is interesting that the overall convergent values of RMSD for the T2 models exhibited lower deviation than those for the T1 models.

Fig. 2(a) and (b) shows that the order of convergence times and RMSD values for each model were similar for the different binding types (T1 and T2), and followed the order: M1 > WT1 > M41 > M31 > WT2. The order of RMSD in the A β -tau mixtures has the same tendency as in a previous study by Miller *et al.*, which was performed with only tau models.^{41,42} From their RMSD results, the low distance order of M1 > M41 > M31 > WT was obtained. Considering the different binding directions

applied in this study (*i.e.*, T1 and T2), our RMSD results were reliable compared with the results obtained by Raz *et al.*⁴¹ The convergent values and their order were mainly caused by the deletion of the lysine residue at position 280. In previous research by Raz *et al.* and Lee *et al.*, the mutated residues effected structure stabilities.^{41,54} Those researchers reported that deleting or mutated the lysine residue not only changed the mutated tau protein conformations, but also changed convergence. For instance, Lee *et al.* investigated the effect of the substitution of glutamine for lysine in tau proteins (*i.e.*, the Q2K model) using a 50 ns equilibrium MD.⁵⁴ From their results, the RMSD convergence tendency of Q2K was faster and had a lower value than the wildtype tau structures.

We observed that the various kinds of A β -tau mixtures were stable after the 20 ns equilibrium simulations. The different binding types for the mixtures showed that the T2 models were more stable than the T1 models, as supported by the RMSD and conformational results. From the RMSD results, we determined that deletion of lysine at position 280 altered the structural conformations and their characteristics. In particular, the proline residue in M31T1 caused more instability than in M41T1. Furthermore, the interior or exterior location of the valine residue also had an effect on the stability of the structures, as shown by computing the differences between the WT1T1 and WT2T1 models. The results from the wildtype (WT) and A β -mutated tau mixtures provided insight into the hydrophobicity, and the charged amino acids altered the stability of each model. The M1 model had higher structural stability than the other models owing to the loss of the charged amino acid (*i.e.*, the lysine residue). Moreover, we observed that, in comparing WT1T1 and WT2T1, the interior location of the valine residue enhanced the structural hydrophobicity and the resulting structural stability.

3.2. Structural characteristics of the A β -tau mixtures

Previous computational studies on homogeneous and heterogeneous amyloids have revealed that the number of inherent hydrogen bonds in a proteinaceous structure is related to its structural stability and mechanical characteristics.^{55–59} Specifically, several recent studies have investigated the impact of end-terminus fluctuation on structural stability.^{60,61} It is also known

that mutations in the CHC regions, the salt-bridge (*i.e.*, A β), and the partition hydrophobic residue (*i.e.*, hIAPP) of amyloids not only affect their fluctuation, but also change their structural characteristics.³⁰

Therefore, we also computed the number of hydrogen bonds for a comparison of the structural characteristics of the WT and mutated models. The different mutated models (*i.e.*, M1, M31, and M41 based on T1 and T2) were also investigated for their impact on the different end-termini, such as the hydrogen-bonding interaction of each A β -mutated tau model. As shown in Fig. 3(a) and 5(a), the hydrogen bond results suggested that all of the heterogeneous mixtures had a common theme in that they were favorable for maintaining the oligomeric structure. Also, the measured number of hydrogen bonds in our A β -tau mixtures for T1 were similar to the values for previous heterogeneous A β and tau protein studies by Miller *et al.*⁴¹ As shown in Fig. 3(a), for the T1 models the order of the number of hydrogen bonds followed the RMSD results of Fig. 2(b). For the other binding types, which were T2 models, we saw a different number of hydrogen bonds compared with the T1 model. Due to the different structural composition of T1 and T2 based on interfacial direction of each A β and tau, T2 model has more number of hydrogen bonds than T1 model. To be more specific, as shown in Fig. S2(c),[†] T2 models have more inter salt-bridge interaction between each A β and tau than T1 models, while T1 models have intra salt-bridge interaction. The inter salt-bridge for A β and tau, which are described at Fig. S2(c),[†] seemed to induce the T2 models have more structural stabilities, and more number of hydrogen bonds. However, the results looked similar to the RMSD values shown in Fig. 2(b) and (c). The T2 models had a higher number of inherent hydrogen bonds than the T1 models; this was similar to the RMSD results for the T2 models, which were structurally more stable than the T1 models. The order of results was similar to that obtained from the RMSD results for the T1 binding models. This order was also comparable to the previous mutated tau study by Raz *et al.*⁴¹ The structural characteristics arising from mutation and residue variation of the tau structures appeared to alter the structural conformation, stability, and characteristics.

These structural stabilities of the heterogeneous A β -tau mixtures were also confirmed by the molecular mechanics (MM) energies. After the equilibrium MD simulation, we measured the MM energies of the WT and mutated models for two different binding types (T1 and T2). Subsequently, we found that the formation of A β -tau mixtures was exothermic and thermodynamically stable. As shown in Tables 1 and 2, we found that all the MM energies were approximately $-500\,000\text{ kJ mol}^{-1}$. The MM energy tendencies were different from the hydrogen bonds results. The WT models including T1 and T2 had lower energy values than the mutated models. The variations of MM energies were caused by mutation and variation of the end residues. The order of energies was slightly different to the previous results obtained from the RMSD and the number of hydrogen bonds.^{41,43} The contribution of MM energy to model stability could be low owing to partial fractures of the models affecting the MM energies. Interestingly, even though the M1 model was shorter than the others, the MM energies of M1 including T1 and T2 were larger than those from the other mutated models. They had more inherent hydrogen bonds than the others models, as confirmed in Fig. 3(b) and 5(b). This could be a result of the conformational cross sectional area of the M1 structure's binding region, as shown in Fig. S1 in the ESI.[†] The M1 model had a tendency of closing its end terminus to reduce contact with water molecules. The cross sectional shape of M1, which is shown in Fig. S1,[†] seemed to be more compact than in the other models. That conformational deformation seemed to cause the increase in the number of inherent hydrogen bonds, and the closed-end terminus sustained the structural stability of the interior region. In the case of the M41 model, the hydrophobic residues located around the end terminus appear to have had a dominant role in structural stability. Because the lysine residues located at the N-terminal regions repel each other electrostatically, they induce breakage of the tau layers, as reflected in the lower MM energies. Even though the cleavage of the tau monomer appears to allow the water molecules to interrupt the interior hydrophobicity, hydrophobic residues in the N- and C-termini of both layers of A β and tau bind and hold each other, so they can maintain the oligomeric form. The M31 model has a proline residue at the N-terminal, which is known

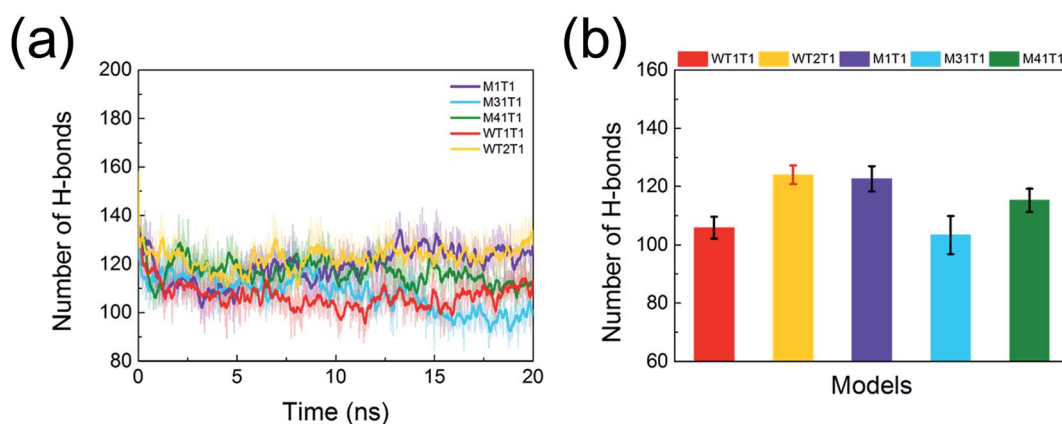


Fig. 3 (a) The number of hydrogen bonds for T1 models are represented at the above graphs. (b) Average the number of hydrogen bonds for the last 5 ns.

Table 1 Molecular mechanics energies of T1 model, such as electro-static energy, van der Waals energy, and total energy for simulated oligomers are given in the table

Binding type	Model	Elec energy (kJ mol ⁻¹)	VdW energy (kJ mol ⁻¹)	Total energy (kJ mol ⁻¹)
T1	WT1	88 394.698 ± 784.44	-660 942.232 ± 1106.65	-504 909.694 ± 468.42
	WT2	86 863.695 ± 757.59	-649 790.225 ± 1066.26	-496 839.325 ± 446.47
	M1	44 195.089 ± 609.09	-331 670.063 ± 858.01	-266 433.269 ± 342.51
	M31	43 762.624 ± 585.29	-327 748.023 ± 829.74	-263 417.592 ± 342.13
	M41	42 468.775 ± 540.90	-319 571.035 ± 799.33	-258 771.240 ± 331.77

Table 2 Molecular mechanics energies of T2 model are given in the table

Binding type	Model	Elec energy (kJ mol ⁻¹)	VdW energy (kJ mol ⁻¹)	Total energy (kJ mol ⁻¹)
T2	WT1	80 818.161 ± 778.66	-605 585.960 ± 1144.64	-464 763.646 ± 451.49
	WT2	85 730.531 ± 816.61	-641 591.569 ± 1104.67	-490 965.083 ± 446.22
	M1	45 076.836 ± 609.19	-338 861.031 ± 857.61	-271 825.954 ± 346.54
	M31	42 669.546 ± 597.89	-320 532.008 ± 809.17	-258 207.197 ± 316.22
	M41	41 828.241 ± 574.70	-314 728.820 ± 812.61	-255 114.379 ± 310.99

as an alpha-helix and beta-sheet breaker. The proline residue in the M31 model revealed the structural instability of M31 through the low number of hydrogen bonds and the high MM/PBSA energy.

Through the number of the hydrogen bonds and the MM energy analysis, we observed that all the WT and mutated models were stable during the 20 ns equilibrium MD simulations. The structural characteristics of the Aβ-tau mixtures were analyzed *via* the hydrogen bond data sets, which had similar characteristics to the conformational and RMSD results. Interestingly, the T2 models had more hydrogen bonds than the T1 models. The different number of hydrogen bonds induced different structural features: the beta sheets in the T2 models seemed to be more parallel than those in the T1 models. An analysis of the MM energies showed that the different thermodynamic characteristics supported the previous structural differences between the WT and mutated models, such as conformation, RMSD, and the number of hydrogen bonds. For example, as shown in Tables 1 and 2, the results showed that the lysine residue in the WT models increased the van der Waals energies and the electrostatic energies of the whole oligomeric mixtures. We not only investigated the structural compositions of the mixtures, but also determined the structural features of heterogeneous Aβ and tau in detail, through the number of hydrogen bonds and MM energy results.

3.3. Mechanical behavior and structural characteristics of mixtures against constant velocity tensile load

From the previous computational studies on amyloids, the structural characteristics of amyloids were investigated through RMSD, the number of hydrogen bonds, MM/PBSA, and other additional parameters.^{30,57} Here, we applied the SMD methods to heterogeneous Aβ-tau mixtures to support the structural characteristics and observe the mechanical responses of applied forces. Generally, SMD simulations of proteins are used to understand mechanical characteristics and properties.^{55,56,62-66} Using the SMD methods on heterogeneous

interfaces between Aβ and tau structures, we compared the structural characteristics between heterogeneous Aβ and tau in detail. After the MD simulations, we obtained the final configurations of the equilibrated states for the WT and mutated models, as shown in Fig. 4(b) and (d) and 6(b) and (d), respectively. SMD simulations (*i.e.*, pulling simulations) were performed to determine the mechanical behavior of the oligomeric mixtures, especially at the heterogeneous interfaces between Aβ and tau. Before analyzing the heterogeneous Aβ and tau mixtures, our magnitude of force reaction from SMD simulation could be compared to previous experimental and computational results. Considering the our Aβ and tau mixtures composed having heterogeneous characteristics, our peak force values of Aβ and tau mixtures were lower than previously reported homogeneous insulin amyloid fibrils, polymorphic hIAPP protofibrils and transthyretin amyloid proteins. But those are in the range of related experimentally measured values.^{55,56,58,65-67}

Interestingly, the time-force graphs were different for the different binding types and residue compositions. As shown in Fig. 4 with the T1 binding models, the time-force results and the pulling trajectories showed that they had double peaks when they were pulled with constant velocity. During the SMD simulation, the Aβ-tau mixtures with binding type 1 (T1) were progressively broken from the C-terminal region at the early stage to the N-terminal regions. Those tendencies were observed for all the T1 models except for M41T1. Because the N-terminus region of M41T1 was already broken during the equilibrium MD simulation, the time-force graphs did not show the first peak. The values of peak force ranged from 200 pN to 800 pN. The first events were observed around a period of 1 ns. The WT1T1 model had a higher peak force than the WT2T1 model, as supported by the MM energy values for WT1T1 and WT2T1. From the MM results in Table 1, we can see that WT1T1 had a more stabilized MM energy than WT2T1. In the case of the mutated model, the peak forces also followed the MM results. For the M41T1 model, we found one peak force

value later than in the remaining models near 1.5 ns. A low peak force for M41T1 of 200 pN was observed. The other models, M31T1 and M1T1, also had peak force results similar to the MM energy results. Interestingly, according to our time–force and pulling trajectories, the crucial agents for the stabilities of heterogeneous A β –tau mixtures were the non-bonding energies, which are van der Waals energies, and electrostatic energies.

However the results for the T2 models, which are plotted in Fig. 6, present a different tendency from the T1 models. The reactions against the tensile force for the T2 models showed a single peak in the time–force graphs. The T2 models were broken from the loop region at the first stage, and the N- and C-termini were separated almost at the same time. Interestingly,

the different fracture behaviors could be supported by the different RMSD results and the different structural characteristics (*i.e.*, hydrogen bonds and MM energies) from the previous analysis sections. Peak force values for the mutated models (*i.e.*, M1, M31, and M41) for T2 were different from those for the T1 models. For the WT models for T2 binding types, the peak force of WT1T2 was higher than for WT2T2, whereas the peak force value results were different from those for RMSD, hydrogen bonds, and MM energies. It was interesting that the structural stability of the oligomeric mixtures did not dominantly affect the peak force in this case.

Thus, through the constant velocity loading simulations, we found that the T1 binding models showed similar behaviors to

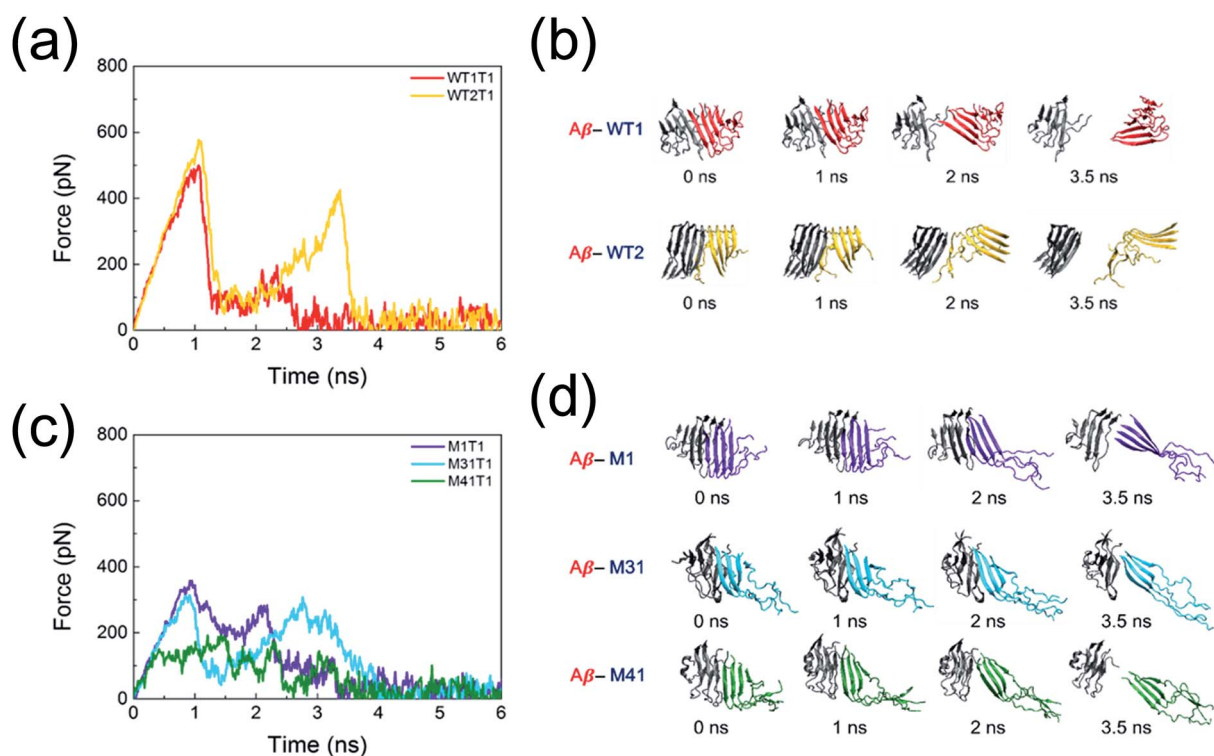


Fig. 4 (a) and (c) are time–force graphs for tensile load with the constant velocity pulling condition. A tendency of them having double peak are observed in both of the graphs. (b) and (d) represents conformational behavior, which are against tensile load for each time.

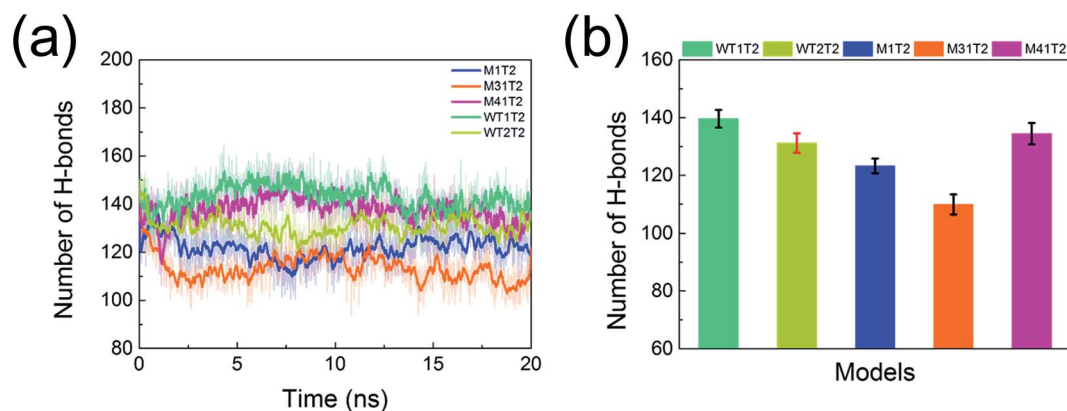


Fig. 5 (a) The number of hydrogen bonds for T2 models are represented. (b) Average the number of hydrogen bonds for the last 5 ns are plotted.

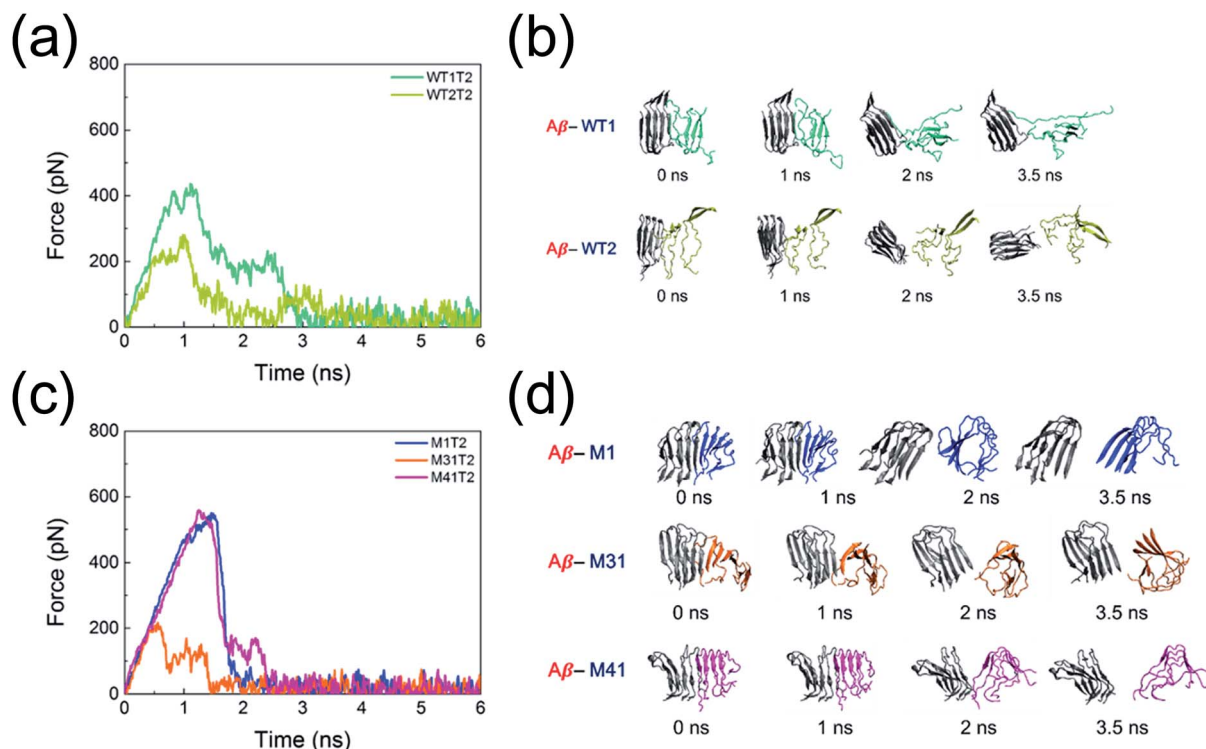


Fig. 6 (a) and (c) are time–force graphs for tensile load with the same pulling condition as the T1 models are. A tendency of them having single peak and step-like shape are observed in the graphs. Just like the Fig. 4, conformational behavior of T2 models are represented at (b) and (d).

the equilibrated MD simulation results for RMSD, conformations, hydrogen bonds, and MM energies owing to the loss of lysine residue and the interior effects of hydrophobic residues. However, the T2 binding model showed different results from the equilibrated MD results because of the different binding direction mechanisms. Using the SMD method on the heterogeneous A β and tau, we confirmed the detailed structural characteristics, which could not be seen in the results from the equilibrium simulations.

3.4. Interacting features for binding types between T1 and T2

In the case of heterogeneous interactions, a comprehensive knowledge of the binding site features is key to understanding the fiber or plaque growth mechanisms of the heterogeneous amyloids. To investigate interaction in the T1 and T2 models, we compared the results of the MM/PBSA and SMD simulations.

In this study, the same residues were considered to observe their role in governing the stability of the heterogeneous WT and mutated tau and A β structures. Previous studies have revealed that interactions between amino acid residues that reside in the interior regions have an important role in maintaining stability.^{55–59} The chemical compositions of structures affect interactions with the surrounding water molecules, and it is known that permeation of water molecules into the interior region can impact the stability of monomers. For example, our computational studies on polymorphic hIAPP revealed that the interior region location of hydrophobic residues altered the

mechanical behavior and properties.^{55–58} The same results were observed in heterogeneous A β , prion, β_2 M, and tau studies.^{30,54,68,69} It was observed that some interior bindings of weak A β and tau models were broken by the permeated water molecules. Subsequently, they caused the lower interior stabilities of mixtures. However, those chemical interactions cannot explain the different results for the T1 and T2 models described previously. The chemical features of the direct binding interactions for each WT and mutated model are represented in Tables S1 and S2.† The chart describes the interaction between layers for a direct comparison between models. However, it shows that there are no notable differences for the different binding types (T1 and T2).

For that reason MM/PBSA was computed to verify those differences in binding energies for each model and binding type, to understand why their binding features were different, even though their chemical binding features were similar for each binding type. To investigate the MM/PBSA energy effectively, the MM/PBSA analysis was separated into MM, PB, and SA sections, as shown in detail in Fig. 7. The solvent accessible surface area (SASA) were computed to determine the hydrophobicity against solvents. The graphs in Fig. 7 suggest that the T1 and T2 models did not have notable differences, except for the M1 models. Only the M1 models (*i.e.*, M1T1 and M1T2) had small surface areas. This is because that they are as short as a single residue, compared with the other models. Individual chemical compositions were similar to each model (WT, M1, M31, and M41), but their interacting features were different for the binding types (T1 and T2). Interestingly, their binding

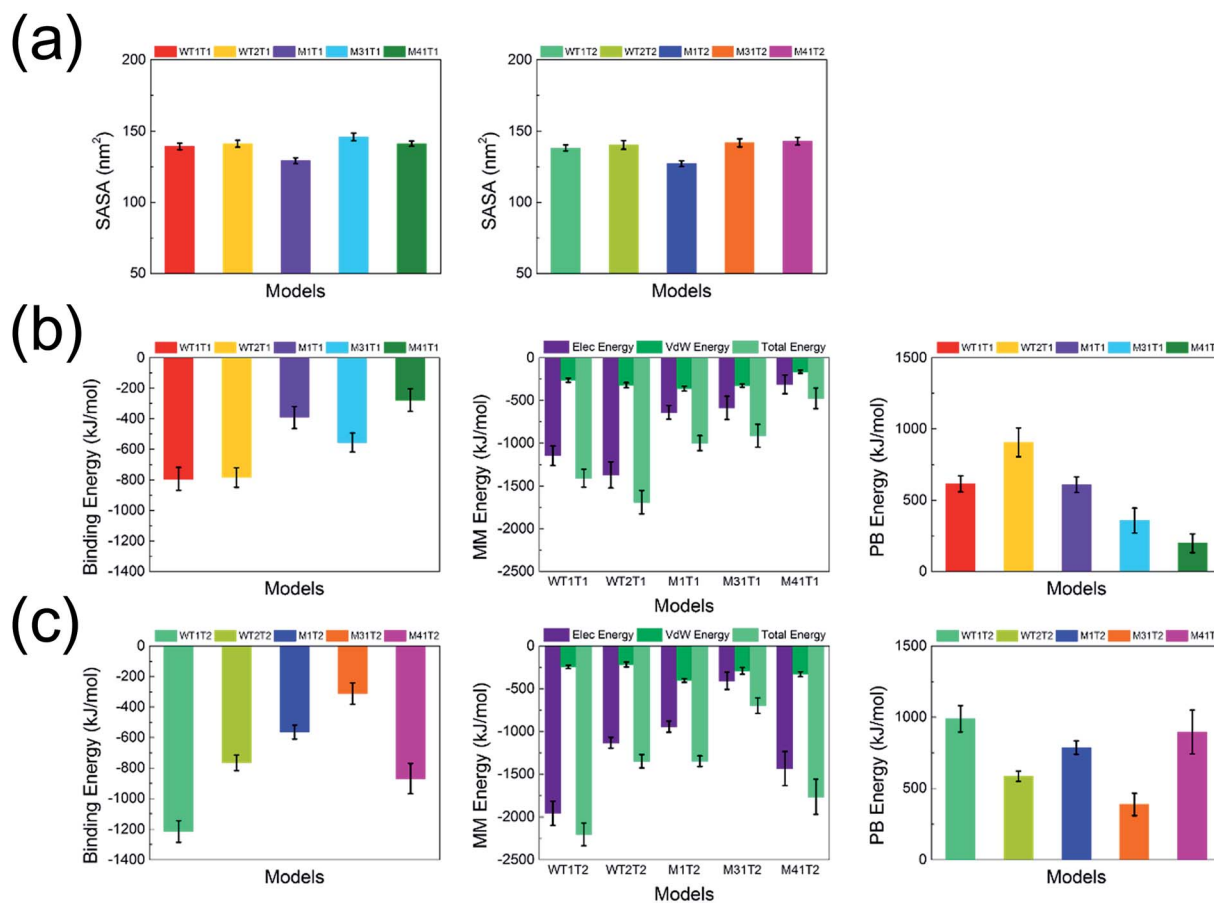


Fig. 7 (a) The solvent accessible surface area (SASA) graphs for T1 (left) and T2 (right). (b) and (c) are binding energy (left), molecular mechanics (MM) energy (middle) and solvation free energy (right) for T1 and T2.

energies showed different values for the binding types. The T2 models had higher binding energies than the T1 models, except for the M31 model, which had similar results for RMSD and the number of hydrogen bond. The only differences between those two binding types were the directions of orientation of interior residues and their stacking orders. Those different conformational compositions induced different binding features, and caused the oligomers to follow different energy reaction pathways for the tensile load in Fig. 4 and 6. Furthermore, the higher binding energy of the T2 models was confirmed through RMSD and the number of hydrogen bonds, as described in the previous sections. The RMSD results for the different binding types, and the results for the number of hydrogen bonds, which are represented in Fig. 3(b) and 5(b) with the average number for a final 5 ns, indicate that the T2 models have more bonds than the T1 models. It was interesting that the conformational stabilities of the A β monomers differed depending on the binding type. Whereas the A β monomers in T2 were well aligned to the fibril axis, those in T1 looked as though their loop regions were dented. Those conformational differences, which are described in Fig. S3 in ESI,[†] could have an impact on the inherent hydrogen bond contents. Moreover, the final shapes of the oligomers provide insight into their elongation.

4. Conclusions

Through combined MD and SMD studies, we investigated the various structural conformations and the structural characteristics of heterogeneous A β and tau mixtures. Specifically, we focused on A β -tau mixtures, with regards to A β monomers as seeds. Lührs model and the mutated effect of R2 tau protein structures by described by Raz *et al.*⁴¹ were used to build simulation models. Moreover, we suggested the different directional elongation features for different binding types for the A β with tau monomers represented as T1 and T2. After 20 ns equilibrium MD simulations, equilibrated WT and mutated simulation models were prepared. Their inherent structural characteristics were different because of deletion of tau's K280 residue. Location effect of the hydrophobic residue (*i.e.*, valine) for tau, and binding models were considered to explain the various interactions of the mixtures. Moreover, after SMD simulation applied to the WT and mutated models, we found that the binding T2 models had different mechanical behaviors compared with the equilibrium results.

Our study provides detailed insights into the structural characteristics of heterogeneous A β -tau mixtures. After conducting equilibrated and steered MD studies, we found that the presence of lysine residue and the location of valine residues

alters the structural conformation and stability. Additionally, from the different T1 and T2 binding models, the structural features of the two different binding types were discussed in order to explain the binding mechanism of the heterogeneous monomers. The results suggest that the heterogeneous interactions of the binding types can produce different stabilized conformations. In particular, the open binding site of A β , where another monomer could be added, showed different structural tendencies for both the T1 and T2 models, and the effect of different shapes of the binding sites should be investigated in the future. These results provide useful insights into understanding how heterogeneous amyloid structures lead to heterogeneous oligomeric amyloid formation mechanisms. Additionally, information about structural stabilities caused by the presence of lysine and the location of valine could shed light on the aggregating features of neurodegenerative disease factors and the elongation and binding mechanisms between monomers.

Acknowledgements

S. N. gratefully acknowledges the Basic Science Research Program, through the National Research Foundation of Korea (NRF) and funded by the Ministry of Science, ICT & Future Planning (MSIP) (No. 2014R1A2A1A11052389).

References

- 1 D. Eisenberg and M. Jucker, *Cell*, 2012, **148**, 1188–1203.
- 2 G. Merlini and V. Bellotti, *N. Engl. J. Med.*, 2003, **349**, 583–596.
- 3 M. B. Pepys, *Annu. Rev. Med.*, 2006, **57**, 223–241.
- 4 L. Adler-Abramovich, L. Vaks, O. Carny, D. Trudler, A. Magno, A. Caflisch, D. Frenkel and E. Gazit, *Nat. Chem. Biol.*, 2012, **8**, 701–706.
- 5 J. Adamcik, J. Jung, J. Flakowski, P. Rios De Los, G. Dietler and R. Mezzenger, *Nat. Nanotechnol.*, 2010, **5**, 423–428.
- 6 N. Mizuno, U. Baxa and A. C. Steven, *Proc. Natl. Acad. Sci. U. S. A.*, 2011, **108**, 3252–3257.
- 7 C. Sachse, N. Grigorieff and M. Fändrich, *Angew. Chem., Int. Ed.*, 2010, **49**, 1321–1323.
- 8 C. Haass and D. J. Selkoe, *Nat. Rev. Mol. Cell Biol.*, 2007, **8**, 101–112.
- 9 C. Soto, *Nat. Rev. Neurosci.*, 2003, **4**, 49–60.
- 10 J. Bieschke, M. Herbst, T. Wiglenda, R. P. Friedrich, A. Boeddrich, F. Schiele, D. Kleckers, J. M. Lopez del Amo, B. A. Grüning, Q. Wang, M. R. Schmidt, R. Lurz, R. Anwyl, S. Schnoegl, M. Fändrich, R. F. Frank, B. Reif, S. Günther, D. M. Walsh and E. E. Wanker, *Nat. Chem. Biol.*, 2012, **8**, 93–101.
- 11 S. R. Collins, A. Douglass, R. D. Vale and J. S. Weissman, *PLoS Biol.*, 2004, **2**, e321.
- 12 W.-F. Xue, A. L. Hellewell, W. S. Gosal, S. W. Homans, E. W. Hewitt and S. E. Radford, *J. Biol. Chem.*, 2009, **284**, 34272–34282.
- 13 Y. Miller, B. Ma, C.-J. Tsai and R. Nussinov, *Proc. Natl. Acad. Sci. U. S. A.*, 2010, **107**, 14128–14133.
- 14 H. Choi, H. J. Chang, Y. Shin, J. I. Kim, H. S. Park, G. Yoon and S. Na, *RSC Adv.*, 2015, **5**, 49263–49269.
- 15 W.-T. Chen, Y.-H. Liao, H.-M. Yu, I. H. Cheng and Y.-R. Chen, *J. Biol. Chem.*, 2011, **286**, 9646–9656.
- 16 P. J. Marek, V. Patsalo, D. F. Green and D. P. Raleigh, *Biochemistry*, 2012, **51**, 8478–8490.
- 17 N. M. Kad, S. L. Myers, D. P. Smith, D. Alastair Smith, S. E. Radford and N. H. Thomson, *J. Mol. Biol.*, 2003, **330**, 785–797.
- 18 N. M. Kad, N. H. Thomson, D. P. Smith, D. A. Smith and S. E. Radford, *J. Mol. Biol.*, 2001, **313**, 559–571.
- 19 A. W. P. Fitzpatrick, G. T. Debelouchina, M. J. Bayro, D. K. Clare, M. A. Caporini, V. S. Bajaj, C. P. Jaronec, L. Wang, V. Ladizhansky, S. A. Müller, C. E. MacPhee, C. A. Waudby, H. R. Mott, A. De Simone, T. P. J. Knowles, H. R. Saibil, M. Vendruscolo, E. V. Orlova, R. G. Griffin and C. M. Dobson, *Proc. Natl. Acad. Sci. U. S. A.*, 2013, **110**, 5468–5473.
- 20 J. T. Nielsen, M. Bjerring, M. D. Jeppesen, R. O. Pedersen, J. M. Pedersen, K. L. Hein, T. Vosegaard, T. Skrydstrup, D. E. Otzen and N. C. Nielsen, *Angew. Chem.*, 2009, **121**, 2152–2155.
- 21 M. R. Sawaya, S. Sambashivan, R. Nelson, M. I. Ivanova, S. A. Sievers, M. I. Apostol, M. J. Thompson, M. Balbirnie, J. J. W. Wiltzius, H. T. McFarlane, A. O. Madsen, C. Riekel and D. Eisenberg, *Nature*, 2007, **447**, 453–457.
- 22 J. Madine, E. Jack, P. G. Stockley, S. E. Radford, L. C. Serpell and D. A. Middleton, *J. Am. Chem. Soc.*, 2008, **130**, 14990–15001.
- 23 L. R. Volpatti, M. Vendruscolo, C. M. Dobson and T. P. J. Knowles, *ACS Nano*, 2013, **7**, 10443–10448.
- 24 J. Dong, J. E. Shokes, R. A. Scott and D. G. Lynn, *J. Am. Chem. Soc.*, 2006, **128**, 3540–3542.
- 25 M. Innocenti, E. Salviati, M. Guidotti, A. Casini, S. Bellandi, M. L. Foresti, C. Gabbiani, A. Pozzi, P. Zatta and L. Messori, *J. Alzheimer's Dis.*, 2010, **19**, 1323–1329.
- 26 D. Noy, I. Solomonov, O. Sinkevich, T. Arad, K. Kjaer and I. Sagi, *J. Am. Chem. Soc.*, 2008, **130**, 1376–1383.
- 27 V. Töugu, A. Karafin, K. Zovo, R. S. Chung, C. Howells, A. K. West and P. Palumaa, *J. Neurochem.*, 2009, **110**, 1784–1795.
- 28 R. Pappaccone, M. A. Pires and M. J. Buehler, *Biochemistry*, 2010, **49**, 8967–8977.
- 29 T. Lühns, C. Ritter, M. Adrian, D. Riek-Loher, B. Bohrmann, H. Döbeli, D. Schubert and R. Riek, *Proc. Natl. Acad. Sci. U. S. A.*, 2005, **102**, 17342–17347.
- 30 H. J. Chang, I. Baek, M. Lee and S. Na, *ChemPhysChem*, 2016, **17**, 425–432.
- 31 M. Lee, H. J. Chang, J. Y. Park, J. Shin, J. W. Park, J. W. Choi, J. I. Kim and S. Na, *J. Mol. Graphics Modell.*, 2016, **65**, 8–14.
- 32 G. Wei and J.-E. Shea, *Biophys. J.*, 2006, **91**, 1638–1647.
- 33 C. Yang, J. Li, Y. Li and X. Zhu, *J. Mol. Struct.: THEOCHEM*, 2009, **895**, 1–8.
- 34 R. Cukalevski, B. Boland, B. Frohm, E. Thulin, D. Walsh and S. Linse, *ACS Chem. Neurosci.*, 2012, **3**, 1008–1016.
- 35 C. Conde and A. Caceres, *Nat. Rev. Neurosci.*, 2009, **10**, 319–332.

- 36 C. Ballatore, V. M. Y. Lee and J. Q. Trojanowski, *Nat. Rev. Neurosci.*, 2007, **8**, 663–672.
- 37 J.-P. Guo, T. Arai, J. Miklossy and P. L. McGeer, *Proc. Natl. Acad. Sci. U. S. A.*, 2006, **103**, 1953–1958.
- 38 K. Ono, R. Takahashi, T. Ikeda and M. Yamada, *J. Neurochem.*, 2012, **122**, 883–890.
- 39 J. Seeliger, F. Evers, C. Jeworrek, S. Kapoor, K. Weise, E. Andreetto, M. Tolan, A. Kapurniotu and R. Winter, *Angew. Chem., Int. Ed.*, 2012, **51**, 679–683.
- 40 D. Pinotsi, A. K. Buell, C. Galvagnion, C. M. Dobson, G. S. Kaminski Schierle and C. F. Kaminski, *Nano Lett.*, 2014, **14**, 339–345.
- 41 Y. Raz, J. Adler, A. Vogel, H. A. Scheidt, T. Haupl, B. Abel, D. Huster and Y. Miller, *Phys. Chem. Chem. Phys.*, 2014, **16**, 7710–7717.
- 42 Y. Miller, B. Ma and R. Nussinov, *Biochemistry*, 2011, **50**, 5172–5181.
- 43 Y. Raz and Y. Miller, *PLoS One*, 2013, **8**, e73303.
- 44 W. Berhanu and A. Masunov, *J. Mol. Model.*, 2012, **18**, 1129–1142.
- 45 M. Zhang, R. Hu, H. Chen, X. Gong, F. Zhou, L. Zhang and J. Zheng, *J. Chem. Inf. Model.*, 2015, **55**, 1628–1639.
- 46 L. Larini, M. M. Gessel, N. E. LaPointe, T. D. Do, M. T. Bowers, S. C. Feinstein and J.-E. Shea, *Phys. Chem. Chem. Phys.*, 2013, **15**, 8916–8928.
- 47 L. Xu, Y. Chen and X. Wang, *J. Phys. Chem. B*, 2014, **118**, 9238–9246.
- 48 V. V. Shvadchak, M. M. A. E. Claessens and V. Subramaniam, *J. Phys. Chem. B*, 2015, **119**, 1912–1918.
- 49 H. J. C. Berendsen, D. van der Spoel and R. van Drunen, *Comput. Phys. Commun.*, 1995, **91**, 43–56.
- 50 R. Kumari, R. Kumar and A. Lynn, *J. Chem. Inf. Model.*, 2014, **54**, 1951–1962.
- 51 S. P. Brown and S. W. Muchmore, *J. Med. Chem.*, 2009, **52**, 3159–3165.
- 52 T. Yang, J. C. Wu, C. Yan, Y. Wang, R. Luo, M. B. Gonzales, K. N. Dalby and P. Ren, *Proteins*, 2011, **79**, 1940–1951.
- 53 J. Kyte and R. F. Doolittle, *J. Mol. Biol.*, 1982, **157**, 105–132.
- 54 M. Lee, I. Baek, H. Choi, J. I. Kim and S. Na, *Biochem. Biophys. Res. Commun.*, 2015, **466**, 486–492.
- 55 M. Lee, H. J. Chang, D. Kim, Y. Lee, H. Suh, N. Ahn, G. Yoon and S. Na, *Biophys. Chem.*, 2015, **199**, 1–8.
- 56 J. I. Kim, M. Lee, I. Baek, G. Yoon and S. Na, *Phys. Chem. Chem. Phys.*, 2014, **16**, 18493–18500.
- 57 G. Yoon, M. Lee, J. I. Kim, S. Na and K. Eom, *PLoS One*, 2014, **9**, e88502.
- 58 M. Lee, I. Baek, H. J. Chang, G. Yoon and S. Na, *Chem. Phys. Lett.*, 2014, **600**, 68–72.
- 59 J. T. Berryman, S. E. Radford and S. A. Harris, *Biophys. J.*, 2011, **100**, 2234–2242.
- 60 M. Lee and S. Na, *ChemPhysChem*, 2016, **17**, 425–432.
- 61 M. Andreassen, K. K. Skeby, S. Zhang, E. H. Nielsen, L. H. Klausen, H. Frahm, G. Christiansen, T. Skrydstrup, M. Dong, B. Schiøtt and D. Otzen, *Biochemistry*, 2014, **53**, 6968–6980.
- 62 S. Max and J. B. Markus, *Nanotechnology*, 2014, **25**, 105703.
- 63 M. Solar and M. J. Buehler, *Nanoscale*, 2012, **4**, 1177–1183.
- 64 B. Choi, G. Yoon, S. W. Lee and K. Eom, *Phys. Chem. Chem. Phys.*, 2015, **17**, 1379–1389.
- 65 M. Lee, J. Kwon and S. Na, *Phys. Chem. Chem. Phys.*, 2016, **18**, 4814–4821.
- 66 M. Lee, H. Choi and S. Na, *J. Nanomater.*, 2016, **2016**, 10.
- 67 J. Smith, T. Knowles, C. Dobson, C. MacPhee and M. Welland, *Proc. Natl. Acad. Sci. U. S. A.*, 2006, **103**, 15806–15811.
- 68 Y. Gwonchan, L. Myeongsang, K. Kyungwoo, K. Jae In, C. Hyun Joon, B. Inchul, E. Kilho and N. Sungsoo, *Phys. Biol.*, 2015, **12**, 066021.
- 69 G. Yoon, Y. Kab Kim, K. Eom and S. Na, *Appl. Phys. Lett.*, 2013, **102**, 011914.